DUPLICATE ALSO

Forecasting Research

Short-Range Forecasting Research Division

Scientific Note No. 18

An Idealized Simulation of the Indian Monsoon using Primitive Equation and Quasi-Equilibrium Models

by

M.H. Mawson and M.J.P. Cullen

August 1990

ORGS UKMO S

National Meteorological Library
FitzRoy Road, Exeter, Devon. EX1 3PB

Meteorological Office (Met O 11)
London Road, Bracknell, Berkshire RG12 2SZ, England

METEOROLOGICAL OFFICE.
Short Range Forecasting Research Division Sci. Note No.18

An idealized simulation of the Indian monsoon using primitive equation and quasi-equilibrium models.

04021190

551.553.21
551.509.313

An Idealised Simulation of the Indian Monsoon using Primitive Equation and Quasi-Equilibrium Models.

M. H. Mawson and M. J. P. Cullen

Short Range Forecasting Research (S1)
Scientific Note No 18

Short Range Forecasting Division,
Meteorological Office,
London Road,
Bracknell,
Berkshire.
RG12 2SZ.

This is an unpublished document and permission to quote from it must be obtained from an assistant director of the above Met. Office division.

Summary.

An idealised simulation of the Indian monsoon is performed using a prescribed heat source representative of the time-averaged latent heating due to convection over India and a simple representation of the East African orography. A quasi-equilibrium model is used to solve this problem in three dimensions on a sphere. The model is shown to be able to simulate the cross-equatorial flow and monsoon circulations driven by this problem and to be in good agreement with parallel integrations carried out with a hydrostatic primitive equation model except in areas affected by orographically forced gravity waves. The solutions given by these time-dependent models are in good agreement with those found by using linearised steady state equations.

1. Introduction.

The view that the "East African Jet (EAJ) is a response to latent heat release in the Indian monsoon" was investigated by Sashegyi and Geisler (1987), henceforth SG, using a linearised steady state model. In their experiment 2 they represented the time-averaged latent heating due to convection in the Indian monsoon as an isolated, prescribed heat source and the East African orography by a solid wall throughout the atmosphere. They showed that with this simple approach they could simulate the monsoon circulation and the cross-equatorial jet. In this paper we repeat that experiment using the same heat source but replacing the solid wall with a more realistic representation of the orography. We solve the problem using two time dependent models. One is a standard primitive equation model, henceforth PE, and the other is a quasi-equilibrium model, henceforth QE. The rationale behind and possible benefits of using quasi-equilibrium dynamics were discussed in Cullen et al(1987).

The study in SG suggested that the main features of the circulation could be determined by the need to balance the pressure perturbation resulting from the heating over Northern India and the confinement of the resulting circulation by the East African highlands. These mechanisms should be described by the quasi-equilibrium model, which assumes that the atmosphere is in a minimum energy state, with respect to a certain class of displacements, at any given time and calculates the velocity field required to maintain the minimum energy state in the presence of dynamical or physical forcing. This ensures a unique solution except in areas where air parcels can be interchanged without affecting the total energy of the system. Cullen and Purser(1989) showed that this was the case across the equator. In this study

we add friction to the QE model in the way discussed by Cullen(1989a) which then makes the solution unique. The model in SG can be obtained by linearising either QE or PE equations and including friction. By using the QE model instead of the linear model of SG it is possible to use more realistic orography and to obtain a closer comparison with the observed behaviour. We can therefore address the question of how much of the observed dynamical behaviour can be explained in terms of the minimum energy argument that underlies the QE model. We also compare the solutions with those from a PE model in order to assess the effect of using more complete dynamics in the same idealised problem.

In section 2 we describe the two models, in section 3 we state the problem to be solved and in section 4 we describe the results with our conclusions in section 5.

2. Model Formulations.

Both models are hydrostatic and use $\sigma=p/p_*$ as the vertical co-ordinate where subscript * denotes the value at the surface. The equations are written in terms of spherical polar co-ordinates (λ,μ,σ) where λ is latitude and μ is longitude. The notation is otherwise standard except where explicitly stated.

a) Quasi-Equilibrium model.

The QE equations are described in the absence of friction by Cullen et al (1987) and are derived by formally making the geostrophic momentum approximation in the hydrostatic equations of motion in spherical geometry. When friction is included (see Cullen(1989a)) the momentum is no longer

approximated by its geostrophic value. Instead we refer to the value used as the equilibrium wind.

The QE equations are as follows ;

$$p_* \frac{\partial u_0}{\partial t} + \frac{U}{a\cos\mu}\frac{\partial u_0}{\partial \lambda} + \frac{1}{a}\frac{\partial u_0}{\partial \mu} + W\frac{\partial u_0}{\partial \sigma} - f(V - p_* v_0) - U v_0 \frac{\tan\mu}{a} = \alpha_F (U - p_* u_0) \qquad (1)$$

$$p_* \frac{\partial v_0}{\partial t} + \frac{U}{a\cos\mu}\frac{\partial v_0}{\partial \lambda} + \frac{1}{a}\frac{\partial v_0}{\partial \mu} + W\frac{\partial v_0}{\partial \sigma} + f(U - p_* u_0) + U u_0 \frac{\tan\mu}{a} = \alpha_F (V - p_* v_0) \qquad (2)$$

$$p_* \frac{\partial \theta}{\partial t} + \frac{U}{a\cos\mu}\frac{\partial \theta}{\partial \lambda} + \frac{1}{a}\frac{\partial \theta}{\partial \mu} + W\frac{\partial \theta}{\partial \sigma} = p_* Q(\lambda,\mu,\sigma) - p_* \alpha_N (\theta - \theta_{ref}) \qquad (3)$$

$$\frac{\partial}{\partial \sigma}\left(\frac{\partial p}{\partial t}\right) + \frac{1}{a\cos\mu}\left[\frac{\partial}{\partial \lambda}\left(\frac{\partial (pu)}{\partial \sigma}\right) + \frac{\partial}{\partial \mu}\left(\frac{\partial (pv\cos\mu)}{\partial \sigma}\right)\right] + \frac{\partial}{\partial \sigma}\left(\frac{\partial (pw)}{\partial \sigma}\right) = 0$$

which reduces to

$$\frac{\partial p_*}{\partial t} + \frac{1}{a\cos\mu}\left[\frac{\partial U}{\partial \lambda} + \frac{\partial (V\cos\mu)}{\partial \mu}\right] + \frac{\partial W}{\partial \sigma} = 0 \qquad (4)$$

$$-f u_0 = \frac{1}{a}\frac{\partial \phi_*}{\partial \mu} + \frac{1}{a} C_p \sigma^{\kappa} \theta \frac{\partial \pi}{\partial \mu} + \alpha_F v \qquad (5)$$

$$f v_0 = \frac{1}{a\cos\mu}\left[\frac{\partial \phi_*}{\partial \lambda} - C_p \sigma^{\kappa} \theta \frac{\partial \pi}{\partial \lambda}\right] + \alpha_F u \qquad (6)$$

$$-R\sigma^{\kappa-1}\theta\,\pi = \frac{\partial \phi}{\partial \sigma} \qquad (7)$$

where $(U,V,W) = p_*(u,v,w)$ and $w = \partial\sigma/\partial t$, Q is the heating function described in section 3, α_N and α_F are relaxation time-scales for the Newtonian cooling and friction respectively. u_0 and v_0 are the equilibrium wind components in the λ

and μ directions, $\pi=(p_*/1000)^{\kappa}$ is the Exner function where $\kappa=R/C_p$, and a is the radius of the earth. We can eliminate ϕ from equations (5) and (6) by using (7) giving

$$f\frac{\partial u_0}{\partial\sigma} = \frac{\pi R\sigma^{\kappa-1}}{a}\frac{\partial\theta}{\partial\mu} - \frac{C_p\sigma^{\kappa}}{a}\frac{\partial\theta}{\partial\sigma}\frac{\partial\pi}{\partial\mu} - \frac{\partial(\alpha_F v)}{\partial\sigma} \qquad (8)$$

$$f\frac{\partial v_0}{\partial\sigma} = -\frac{\pi R\sigma^{\kappa-1}}{a\cos\mu}\frac{\partial\theta}{\partial\lambda} + \frac{C_p\sigma^{\kappa}}{a}\frac{\partial\theta}{\partial\sigma}\frac{\partial\pi}{\partial\lambda} + \frac{\partial(\alpha_F u)}{\partial\sigma} \qquad (9)$$

The solution procedure is a predictor/corrector method based on that suggested by Meek and Norbury(1984) and is described in more detail by Cullen(1989b). The first four equations allow us to step the variables u_0, v_0, p_* and θ forward in time giving provisional values at the new time level. This still requires the determination of u and v at the new time level. This is done by noting that equations (5-6) applied at the surface and (8-9) at the levels above the surface will not be exactly satisfied by the provisional values at the new time level. We therefore solve these equations to obtain the corrections to u and v needed to satisfy them.

$$f\Delta u_0 + 1/a\ C_p\ \sigma^{\kappa}\ \Delta\theta\ \partial\Delta\pi/\partial\mu + \alpha_F\Delta v = D_* \qquad (10)$$

$$f\Delta v_0 - 1/(a\cos\mu)\ C_p\ \sigma^{\kappa}\ \Delta\theta\ \partial\Delta\pi/\partial\lambda - \alpha_F\Delta u = E_* \qquad (11)$$

$$f\frac{\partial\Delta u_0}{\partial\sigma} - \frac{\Delta\pi R\sigma^{\kappa-1}}{a}\frac{\partial\Delta\theta}{\partial\mu} + \frac{C_p\sigma^{\kappa}}{a}\frac{\partial\Delta\theta}{\partial\sigma}\frac{\partial\Delta\pi}{\partial\mu} + \frac{\partial(\alpha_F\Delta v)}{\partial\sigma} = D_k \quad (2\le k\le N) \qquad (12)$$

$$f\frac{\partial\Delta v_0}{\partial\sigma} + \frac{\Delta\pi R\sigma^{\kappa-1}}{a\cos\mu}\frac{\partial\Delta\theta}{\partial\lambda} - \frac{C_p\sigma^{\kappa}}{a}\frac{\partial\Delta\theta}{\partial\sigma}\frac{\partial\Delta\pi}{\partial\lambda} - \frac{\partial(\alpha_F\Delta u)}{\partial\sigma} = E_k \quad (2\le k\le N) \qquad (13)$$

D_* E_* , D_k, and E_k are the residuals obtained from equations (5),(6),(8) and (9) respectively and N is the number of model levels. Equations (10) and (12)

are solved in (μ,σ) slices with the corrections Δu_0, $\Delta\theta$ and $\Delta\pi$ written in terms of Δv by using the 2-dimensional (μ,σ) version of equations (1),(3) and (4). The resulting equations are elliptic provided that the potential vorticity is non-negative. The finite-difference scheme is not valid in the presence of discontinuities so exact solution of these equations for the u and v correction leads to instability. Cullen(1989b) showed by comparison with a lagrangian model valid at discontinuities that a satisfactory solution to the problem could be obtained by approximating (10)-(13) by a reduced system which is elliptic provided that

$$\partial\theta/\partial\sigma < 0 \quad \text{and} \quad -\partial u_0/\partial\mu + af > 0 \qquad (14)$$

which are the conditions that the data is statically and inertially stable. These conditions are enforced by modifying the data before solving equations (10) and (12). We obtain our provisional value of v at the new time level by adding on Δv calculated from this reduced system. The solution procedure may need to be iterated, but if iterated to convergence will again produce instability in the presence of discontinuities. A small fixed number of iterations is therefore used. The solution obtained this way may still diverge if the potential vorticity, defined as the determinant of a function $P = \phi + \frac{1}{2} f^2(x^2 + y^2)$, is negative. This occurs infrequently at a few points and may be avoided by increasing the frictional damping in the vicinity of these points. In reality the QE equations are not a valid approximation to the primitive equations in such regions and the friction is being used to parameterize the dissipative unbalanced motion which is likely to occur there. Periodic boundary conditions are applied in the μ direction and we set W=0 at σ=0 and 1. A similar approach is applied in the (λ,μ) plane using equations (11) and (13) to find the correction Δu with ellipticity conditions

$$\partial\theta/\partial\sigma < 0 \quad \text{and} \quad \partial v_0/\partial\lambda + af\cos\mu > 0. \qquad (15)$$

The three dimensional problem is solved by an Alternating Direction Implicit (ADI) method in which the (μ,σ) and (λ,σ) problems are solved alternately.

The theory behind the QE model (Cullen and Purser(1989)),in the absence of friction, shows that there is a unique $\underline{U}$ field which maintains the atmosphere in a minimum energy state. This computational procedure is an iterative method of calculating $\underline{U}$. In practice it is found that some smoothing of the iteration is required to improve the convergence of the ADI on small horizontal and large vertical scales. This is done by averaging on a σ-surface Δu and Δv at point i as follows;

$$\Delta u_i = .5 * (\Delta u_i + .2 \sum_{j=i-2}^{i+2} \Delta u_j) \qquad (16)$$

with Δv being treated similarly.

The variables are held on a staggered grid as shown in fig.1. The grid staggering is that which appears naturally when the equations are written out using centred finite-differencing.

b. Primitive Equation model.

The basic equations are ;

$$\frac{\partial u}{\partial t} + \frac{u}{a\cos\mu}\frac{\partial u}{\partial\lambda} + \frac{v}{a}\frac{\partial u}{\partial\mu} + w\frac{\partial u}{\partial\sigma} - (f + \frac{u\tan\mu}{a})v + \frac{1}{a\cos\mu}\frac{\partial\phi}{\partial\lambda} + Cp\sigma^{\kappa}\theta\frac{\partial\pi}{\partial\lambda} =$$

$$-\alpha_F u \qquad (17)$$

$$\frac{\partial v}{\partial t} + \frac{u}{a\cos\mu}\frac{\partial v}{\partial \lambda} + \frac{v}{a}\frac{\partial v}{\partial \mu} + w\frac{\partial v}{\partial \sigma} + (f + \frac{u\tan\mu}{a})v + \frac{1}{a}\frac{\partial \phi}{\partial \mu} + C_p\sigma^{\kappa}\theta\frac{\partial \pi}{\partial \mu} =$$

$$-\alpha_F v \qquad (18)$$

$$\frac{\partial \theta}{\partial t} + \frac{u}{a\cos\mu}\frac{\partial \theta}{\partial \lambda} + \frac{v}{a}\frac{\partial \theta}{\partial \mu} + w\frac{\partial \theta}{\partial \sigma} = Q(\lambda,\mu,\sigma) - \alpha_N(\theta - \theta_{ref}) \qquad (19)$$

$$\frac{\partial p_*}{\partial t} + \frac{1}{a\cos\mu}\left[\frac{\partial U}{\partial \lambda} + \frac{\partial (V\cos\mu)}{\partial \mu}\right] + \frac{\partial W}{\partial \sigma} = 0 \qquad (20)$$

$$-R\sigma^{\kappa-1}\theta\pi = \frac{\partial \phi}{\partial \mu} \qquad (21)$$

where the notation is the same as used in 2a. The method of solution is that used in the U.K. Met. Office operational model, see Bell and Dickinson(1987) for details, and is based on the split-explicit scheme of Gadd(1978). The equations are solved on a B-grid as shown in fig. 2, note the different vertical as well as horizontal staggering between the grids in figs.1 and 2.

3. Problem Posed.

We consider the same problem as in SG experiment 2. The reference potential temperature profile is that of a typical tropical atmosphere and is taken from Stevens et al(1977) with

$$\theta_{ref}(p) = (p_0/p)^{\kappa}\,\Gamma/\kappa + \theta_0 - \Gamma/\kappa \qquad (22)$$

where p_0 and θ_0 are the reference surface pressure and potential temperature values set to 1000 mb and 300K respectively. Γ is the mean static stability

which is set following Stevens et al(1987) as $R\Gamma/g = 620$.

The time averaged latent heating due to convection is represented by an idealised heating function as in SG

$$Q(\lambda,\mu,\sigma) = B(p)\ \exp[-\{(\lambda-\lambda_0)/\lambda_w\}^2]\ \exp[-\{(\mu-\mu_0)/\mu_w\}^2] \qquad (23)$$

where (λ_0,μ_0) are the co-ordinates of the heat-source centre and λ_w , μ_w are the half-widths of the function. The vertical dependence is

$$B(p) = Q_c \ \frac{(p-p_t)\ (p-p_a)\ (p-p_b)}{(p_m-p_t)\ (p_m-p_a)\ (p_m-p_b)} \qquad p_t \le p \le p_b \qquad (24)$$

$$= 0 \qquad \text{otherwise}$$

where p_b=908mb is the pressure at cloud bottom, p_t=140mb is the pressure at cloud top and p_a=932mb is chosen so that the heating is a maximum of Q_c at p_m=400mb. Setting Q_c to 6K per day provides an integrated latent heating which corresponds to a rainfall rate of 1 cm per day. The parameters in (23) are λ_0=82.5°E, μ_0 = 24°N, λ_w= 22.5° , μ_w = 12°, which are the same as in SG except for λ_0. The 11 model levels are chosen differently for each model in such a way that the differences in heating profile are minimised. The only major difference between the analytic profile and the discrete one used in our models is at the top where the profile we have used adds slightly more heat, see fig. 3.

The East-African orography is represented as a 2-gridlength ridge in the east-west direction with the top at 800mb extending from 15°N to 15°S and located 48° west of the heat-source centre. The frictional and Newtonian cooling relaxation timescales α_F and α_N are set equal to 5 days^{-1}. The initial conditions are $\theta=\theta_{ref}$ everywhere , p_*=1000mb, ϕ_*=0, except over the orography

where p_*=800mb and ϕ_* is set by applying equation (21). The wind components are set to zero everywhere. The models are run at 3°x3.75° resolution giving a grid-length of approximately 400km near the equator.

4. Results.

On some of the figures referred to in this section a coastline is included as an aid to visualizing the solution. All the results in this section are for T+120. At this time the solutions have not quite reached their equilibrium states but the differences between these solutions and the equilibrium ones are small except for areas where numerical noise is a problem. The noise caused by the numerical schemes can be alleviated but different methods have to be employed in the two models making it difficult to compare them exactly. Only one iteration per timestep was required in the QE model. As stated in SG the damping timescales we have chosen lead to an e-folding width for the jet of approximately 100km so with our 400km resolution we will not be able to reproduce the wind maxima they obtained, however the broader scale features should still be comparable.

Figs 4a. and 4b. show the mean sea level pressure field for the QE and PE models respectively. Both models generate a low with central pressure of about 992mb with the PE model approximately .5mb lower when the grid-point values are inspected. The centre of the depression is in the same place in both models and is about 3°N and 12°W of the centre of the heat source marked on the figures as Q. The position is in good agreement with SG although they obtained a central pressure of 989mb. The difference in values between the models reflect their different gradient wind relations. The neglect of the non-linear terms in SG probably accounts for most of 3mb difference between

their solutions and the ones obtained here with increased resolution accounting for the rest.

The surface wind field for the QE model, fig 5a, shows generally weak cross-equatorial flow with a narrow region of greatly enhanced flow next to the orography. Also noticeable is a broader region of enhanced flow around the northern end of the orography and a strong westerly flow over the orography exactly on the equator. The enhanced flow around the northern end of the orography and the low-level cross-equatorial jet are both caused by the blocking effect of the mountain which forces the air needed to satisfy the inflow into the depression to be channelled both along the side and accelerated around the northern end of the orography. The increased flow across the orography on the equator is caused by cold air damming against the side of the mountain. The cold air builds up until it reaches the top of the orography then it spills over producing a strong down slope wind. Similar features can be seen in the PE model, fig 5b, although here the flow around the northern end of the orography is stronger and the enhanced cross-equatorial jet is weaker and broader than in the QE model. To examine the cross-equatorial jet more closely we consider cross-sections of v along $2^{\circ}N$. In the QE model, fig 6a, we can see a narrow jet which extends from the ground to about half the orographic height with the maximum value of 8 ms^{-1} being obtained at the ground. Above this there is a small negative and then a small positive, the existence of which is probably due to finite-difference errors. In the PE model, fig 6b, we see a much weaker jet which extends for the whole depth of the mountain with an almost uniform velocity. The maximum value is $4ms^{-1}$ near the top. The negative value running along the top of the orography is again a finite-differencing problem. SG obtained a jet maxima next to the ground which is in better agreement with the QE solution than the

PE although neither model can reproduce their maxima of $36ms^{-1}$ which was achieved with a 50km resolution. The different vertical structure of the jet maxima in the PE model is not understood although the extra depth of the jet compensates for the reduced strength and mass transfer across the equator is similar to the QE model. The more realistic orography in these models has removed the spurious northerly jet present in the upper atmosphere in SG and replaced it with a weak large scale flow as can be seen for the QE model in fig 7a although still possessing a small area of enhancement near the orography. The PE model ,fig 7b, also possesses this enhancement in the same place along with orographic gravity waves whose presence, though highly noticeable, has little impact on the main solution.

The net heating of both models as well as the conservation properties of the finite difference schemes can be compared by looking at the mass-flux in both the zonal and meridional directions. Following SG we define the mass-flux streamfunction $M(\lambda,p)$ in the zonal plane integrated from equator to pole and from a reference pressure to pressure p as

$$M(\lambda,p) = -a/g \int_{p_r}^{p} \int_{0}^{\pi/2} u(\lambda,\mu,p)\, d\mu\, dp$$

where p_r is the reference surface pressure. We define similarly the mass-flux streamfunction $M(\mu,p)$ in the meridional plane integrated around the globe as

$$M(\mu,p) = -a/g \int_{p_r}^{p} \int_{0}^{2\pi} v(\lambda,\mu,p)\, d\lambda\, dp$$

The interpretation of these quantities is that the direction of the contours of the mass-flux streamfunction show the direction of the mass transport whilst the difference in magnitude between any two contours gives the magnitude of the mass transport. The meridional mass-flux streamfunction is shown in figs 8a and 8b for the QE and PE models respectively. The two models agree very well with the maximum value being at the same height and latitude.

The two models compare well with SG who had a net transfer of 24.5 x $10^{12}gs^{-1}$ which in the PE was 25 x $10^{12}gs^{-1}$ and 23 x $10^{12}gs^{-1}$ in the QE. In the zonal streamfunction , QE fig 9a and PE fig 9b, the maxima in both models is again located at the same height with approximately the same value but about 20° apart. This difference in position is probably due to the extra strength in the flow around the northern end of the orography in the PE model. The difference in the maxima of 3 x $10^{12}gs^{-1}$ between the QE and PE models almost exactly cancels the difference in the meridional direction showing that both models have almost identical forcing. Again both models are very close to the value in SG of 47 x $10^{12}gs^{-1}$.

5. Summary and Conclusions.

Both QE and PE models demonstrate the ability to simulate the EAJ and monsoon circulation in response to this simple idealized heat source. They are in good agreement with each and with the linearised study of SG with the main difference being the PE models weaker jet maxima being located away from the surface. The lack of horizontal resolution in our simulations prevented them reproducing the detail and strength of the EAJ seen in SG but the close agreement in the large scale flow seen by looking at the mass-fluxes suggests that increasing the resolution would restore the detail. The removal of the solid wall throughout the depth of the atmosphere used in SG has had little effect on the solution except in removing the spurious return jet seen in the upper air in their simulation.

Observations of the cross-equatorial mass-flux, eg. Findlater(1969) suggest an average value for July of around 89 x $10^{12}gs^{-1}$ between 35°E and 75°E from the surface up to 600mb. The values we obtained here are only about

30% of that, but we are only considering one of the possible forces driving cross-equatorial transport. Further our assumptions about rainfall rate may also be inaccurate with an increase in the rate leading to an increased mass-flux. A large degree of confidence in the value of this rainfall rate is therefore needed before we can evaluate the importance of this mechanism in the driving of the EAJ although we can conclude that this is one type of forcing which will drive the circulation. The main difference in the observed jet structure and the ones obtained in the QE model and in SG is that in reality the maxima occurs away from the surface due to the frictional effects in the atmospheric boundary layer. This effect is not included in either of our models or that used by SG. The PE model has produced a maximum in a position which is in good agreement with observations, the absence of a boundary layer scheme in the model means that not too much weight should be given to the result. Whether this positioning in the PE models is a result of the equations themselves or of the finite-difference method used to solve them can only be answered by applying this problem to a PE model with a different finite-difference solution procedure.

In this test problem we have shown that QE dynamics can simulate an important part of tropical dynamics namely the ability to support cross-equatorial flow. This shows that this type of response to heat sources can be described in terms of an equilibrium between forcing and maintenance of balance requirements. It is then natural to ask whether these dynamics can simulate further important tropical motions such as the 30-60 day oscillation and the Quasi-Biennial Oscillation. This will be the object of future work.

References.

Bell,R.S. and Dickinson,A.	1987	The Meteorological Office operational numerical weather prediction system. Meteor. Office Sci. Paper No 41. H.M.S.O
Cullen,M.J.P., Norbury,J., Purser,R.J. and Shutts,G.J.	1987	Modelling the quasi-equilibrium dynamics of the atmosphere. Q. J. R. Meteorol. Soc. 113, 735-757.
Cullen,M.J.P. and Purser,R.J.	1989	Properties of the Lagrangian semi-geostrophic equations. J. Atmos. Sci. 46, 2684-2697.
Cullen,M.J.P.	1989a	On the incorporation of atmospheric boundary layer effects into a balanced model. Q. J. R. Meteorol. Soc. 115, 1109-1131.
Cullen,M.J.P.	1989b	Implicit finite difference methods for modelling discontinuous atmospheric flows. J. Comput. Phys. 81, 319-348.
Findlater,J.	1969	Interhemispheric transport of air in the lower troposphere over the Western Indian Ocean. Q. J. R. Meteorol. Soc. 95, 400-403.
Gadd,A.J.	1978	A split-explicit integration scheme for numerical weather prediction. Q. J. R. Meteorol. Soc. 104, 569-582.
Meek,P.C. and Norbury,J.	1984	Non-linear moving boundary problems and a Keller box scheme. Siam. J. Numer. Anal. 21, 883-893.

Sashegyi,K.D. and Geisler,J.E. 1987 A linear model study of cross-equatorial flow forced by summer monsoon heat sources. J. Atmos. Sci. 44, 1706-1722.

Stevens,D.E., Lindzen,R.S. and Shapiro,L.J. 1977 A new model of tropical waves incorporating momentum mixing by cumulus convection. Dyn. Atmos. Oceans. 1, 365-425.

List of Figures.

1. QE model grid.

2. PE model grid.

3. Comparison of analytic heating profile with model heating profiles.

4a. QE model, pressure at mean sea level. Contours every 1mb.

4b. PE model, pressure at mean sea level. Contours every 1mb.

5a. QE model, wind vectors at surface.

5b. PE model, wind vectors at surface.

6a. QE model, v-component cross-section at 2°N. Contours every $1ms^{-1}$

6b. PE model, v-component cross-section at 2°N. Contours every $1ms^{-1}$

7a. QE model, v-component at 300mb. Contours every $1ms^{-1}$

7b. PE model, v-component at 300mb. Contours every $1ms^{-1}$

8a. QE model. Zonally integrated meridional mass-flux streamfunction. Contours every $10^{12}gs^{-1}$.

8b. PE model. Zonally integrated meridional mass-flux streamfunction. Contours every $10^{12}gs^{-1}$.

9a. QE model. Meridionally integrated zonal mass-flux streamfunction. Contours every $10^{12}gs^{-1}$.

9b. PE model. Meridionally integrated zonal mass-flux streamfunction. Contours every $10^{12}gs^{-1}$.

Figure 1.

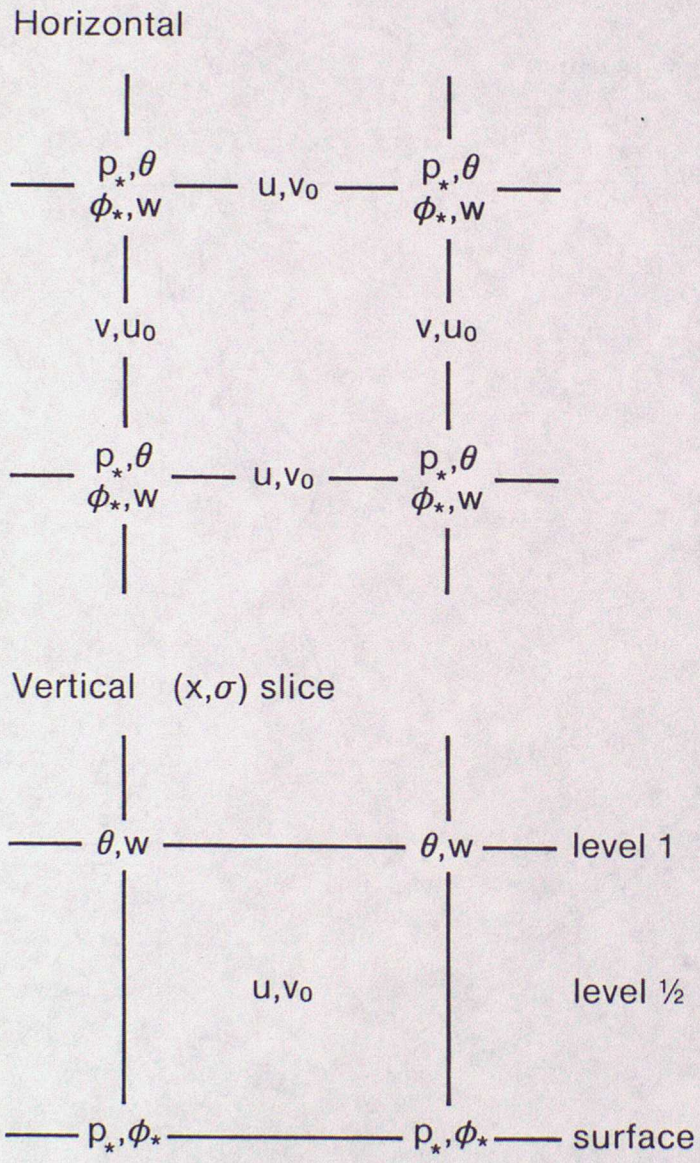

Figure. 2.

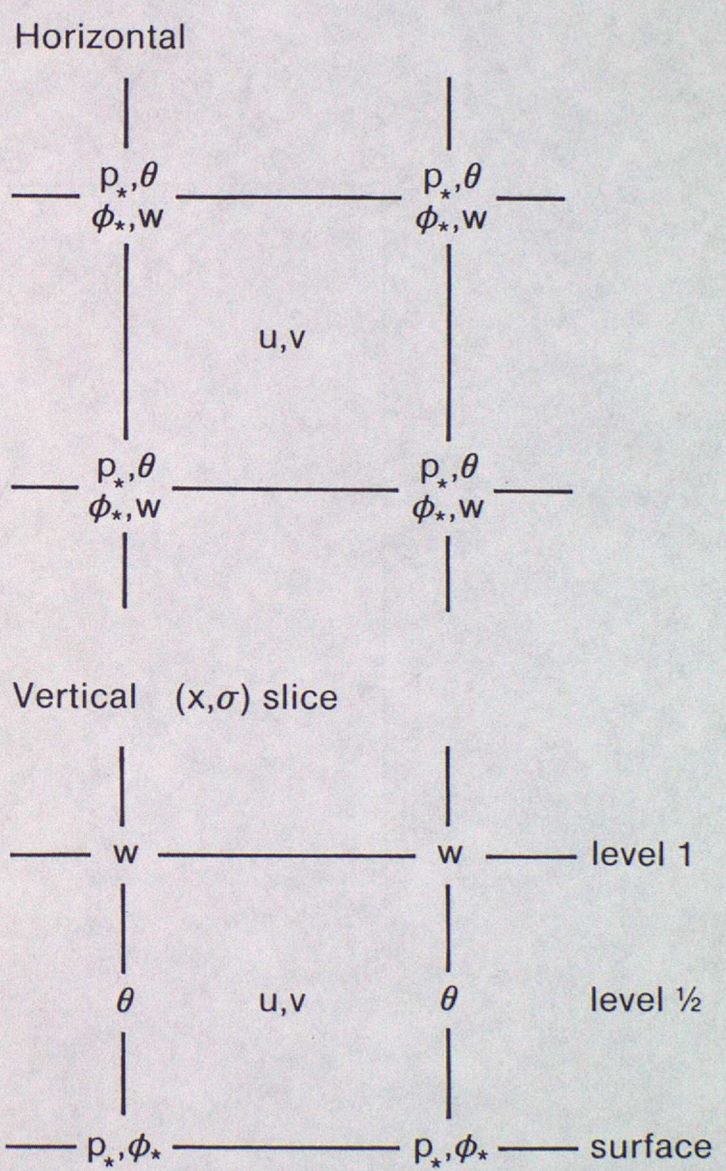

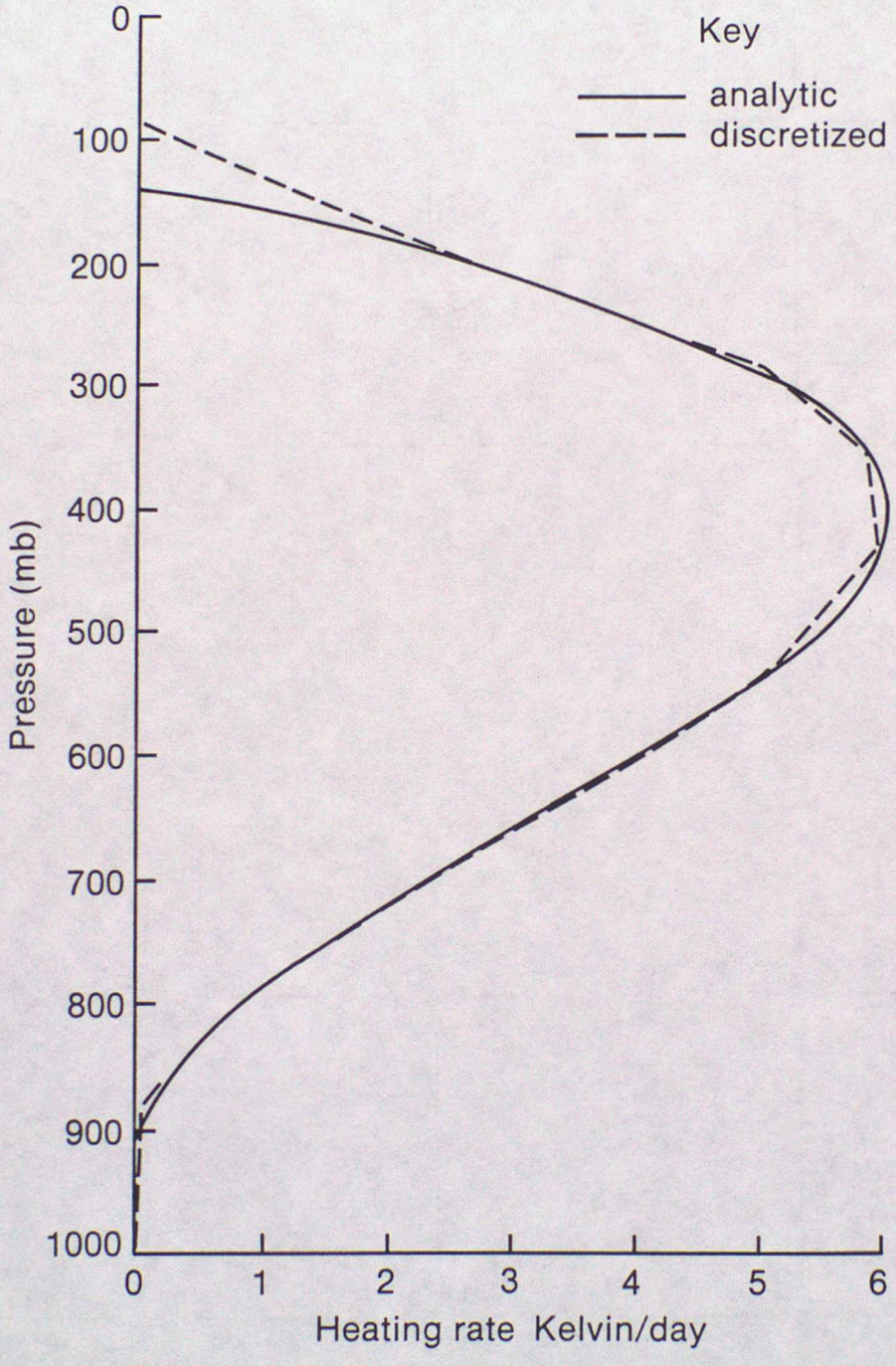
Key
analytic
discretized
Pressure (mb)
0
100
200
300
400
500
600
700
800
900
1000
0
1
2
3
4
5
6
Heating rate Kelvin/day

Figure. 3.

Figure. 4.

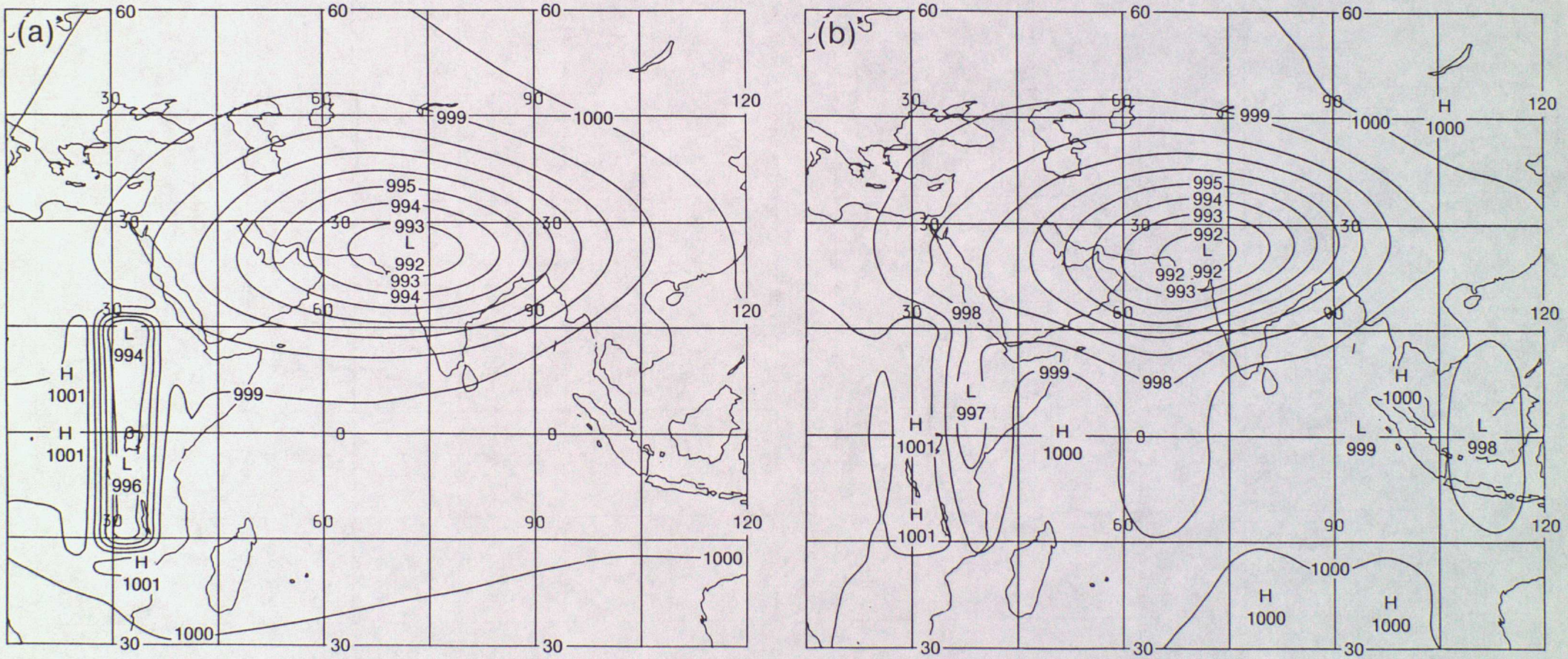
(a)
60
30
0
90
120
999
1000
995
994
993
992
L
H
1001
996
(b)
998
997
1000

Figure. 5.

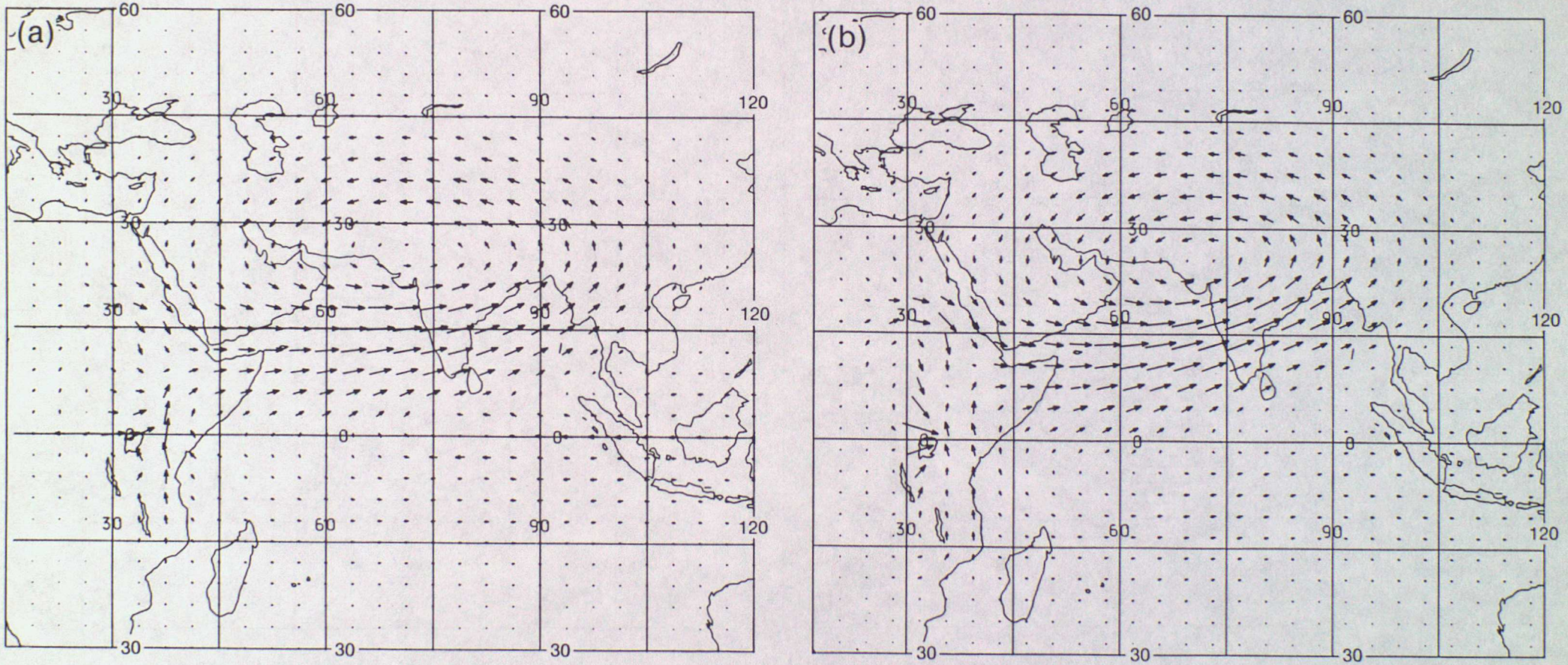

Figure. 6.

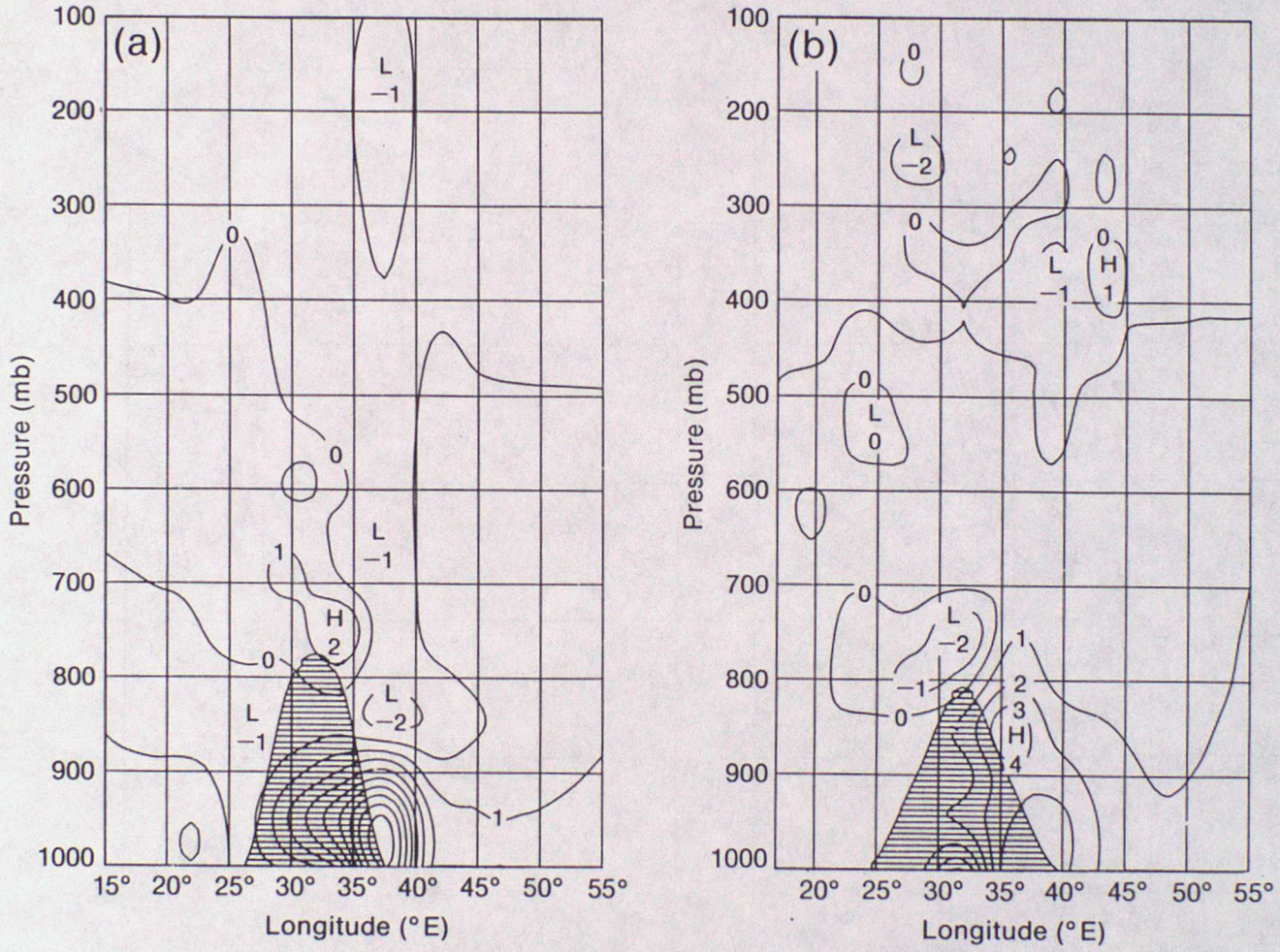
(a)
(b)
Pressure (mb)
100
200
300
400
500
600
700
800
900
1000
15° 20° 25° 30° 35° 40° 45° 50° 55°
20° 25° 30° 35° 40° 45° 50° 55°
Longitude (°E)
L −1
L −2
H 2
H 1
H 4
L 0

Figure. 7.

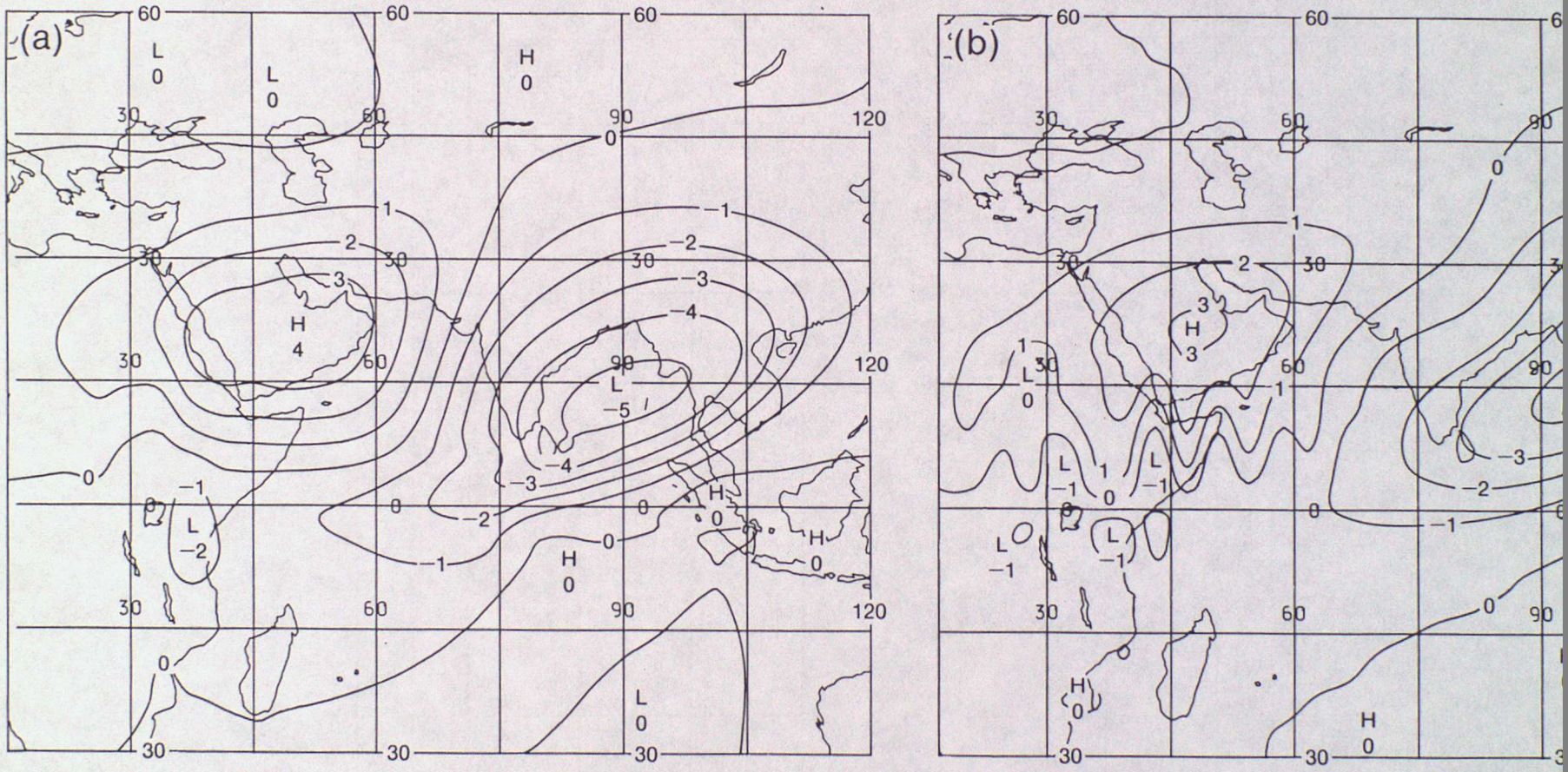

Figure. 8.

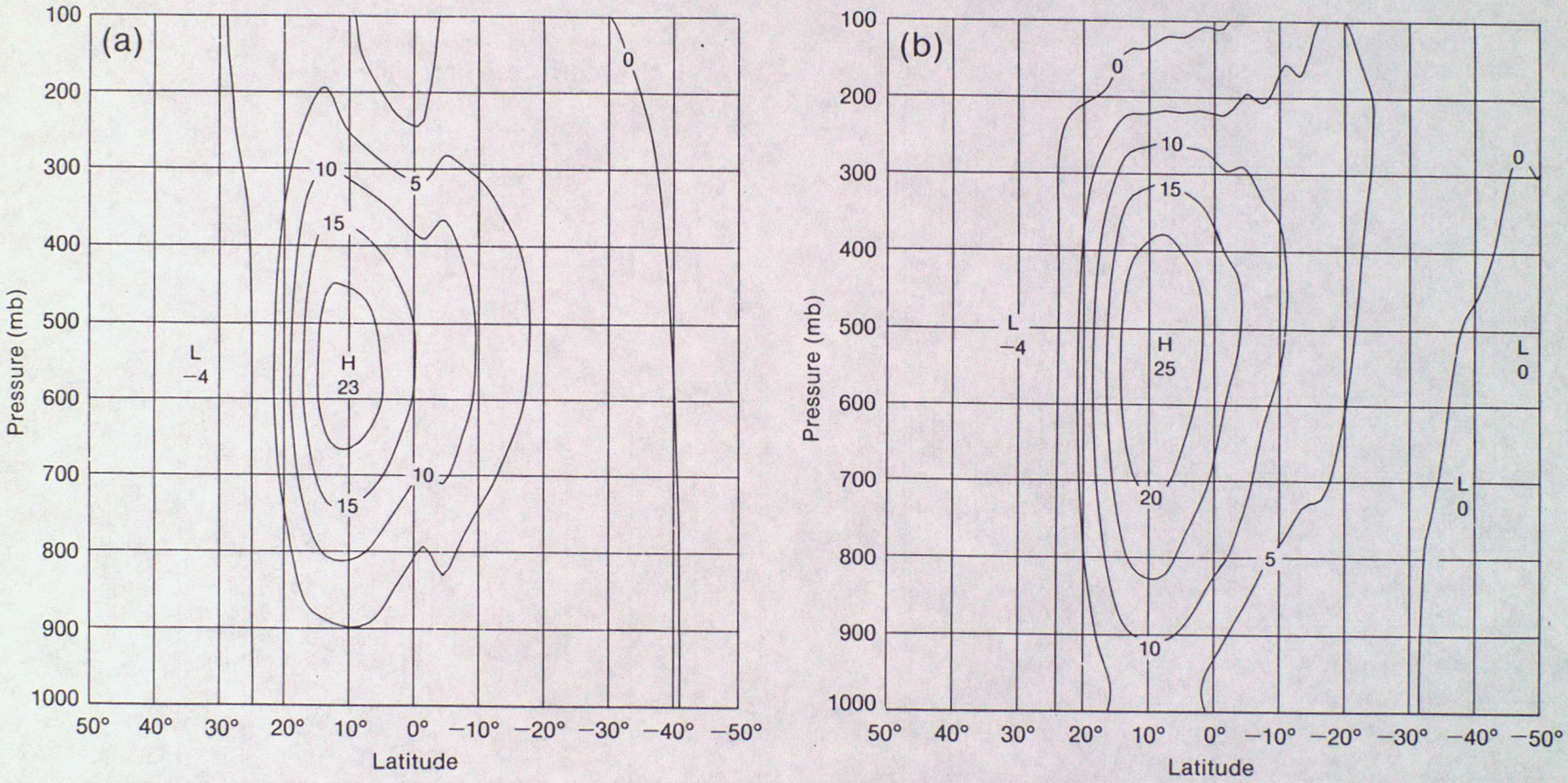
(a)
100
200
300
400
500
600
700
800
900
1000
Pressure (mb)
L
−4
H
23
0
5
10
15
10
15
50° 40° 30° 20° 10° 0° −10° −20° −30° −40° −50°
Latitude
(b)
Pressure (mb)
0
10
15
0
L
−4
H
25
L
0
20
L
0
5
10
Latitude

Figure. 9.

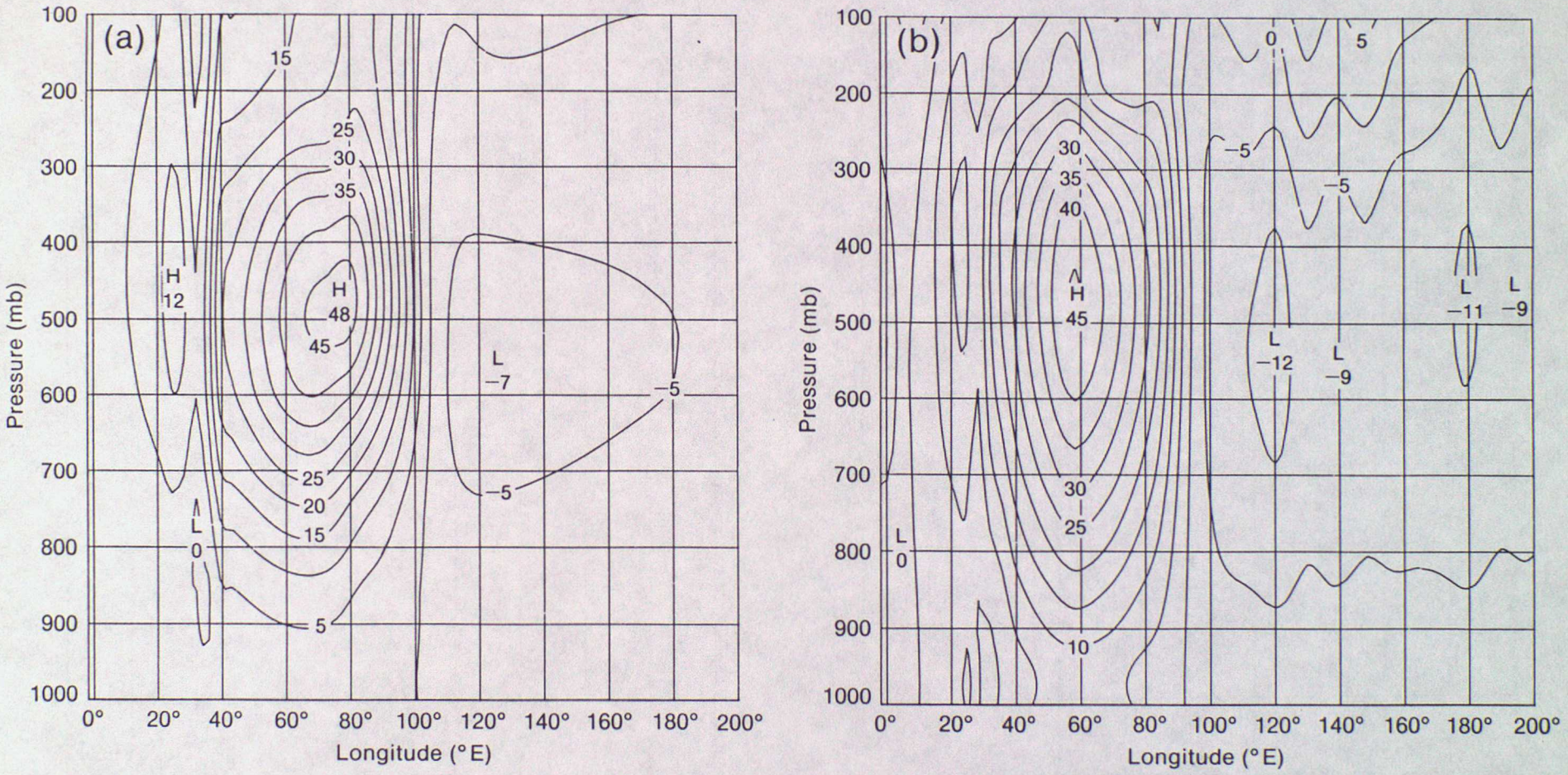
(a)
(b)
Pressure (mb)
Longitude (°E)
100
200
300
400
500
600
700
800
900
1000
0°
20°
40°
60°
80°
100°
120°
140°
160°
180°
200°
H
L
15
25
30
35
12
48
45
−7
−5
25
20
15
0
5
0
5
−5
−5
30
35
40
45
30
25
10
−12
−9
−11
−9

CURRENT SHORT - RANGE FORECASTING RESEARCH SCIENTIFIC NOTES (AUGUST 1990)

The Short- Range Forecasting Research Branch (formerly Met O 11) Scientific Notes which contain information of current use are listed below. The complete set of Scientific Notes is available from the National Meteorological Library on loan, if required.

1. **The theory of periodic solutions of the semi-geostrophic equations.**
R.J. Purser
October 1987

2. **Properties of the partial differential equations governing various types of atmospheric motions and implications for numerical methods.**
M.J.P. Cullen
December 1987

3. **A geometric model of balanced, axisymmetric flows with embedded penetrative convection.**
G.J. Shutts, M. Booth and J. Norbury
February 1988

4. **Implicit finite difference methods for computing discontinuous atmospheric flows.**
M.J.P. Cullen
March 1988

5. **Variational aspects of semi-geostrophic theory.**
R.J. Purser
August 1988

6. **On the incorporation of atmospheric boundary layer effects into a balanced model.**
M.J.P. Cullen
July 1988

7 **Implicit finite difference methods for modelling discontinuous atmospheric flows.**
M.J.P. Cullen
June 1988

8. **An analytical model of the growth of a frontal intrusion.**
M.W. Holt and G.J. Shutts
November 1988

9. **Planetary semi-geostrophic equations derived from Hamilton's principle.**
G.J. Shutts
July 1988

10. **Semi-geostrophic moist frontogenesis in a Lagrangian model.**
M.W. Holt
September 1988

11. **Generalised Lagrangian solutions for atmospheric and ocean flows.**
M.J.P. Cullen, J. Norbury and R.J. Purser
November 1988